Characterisation and evaluation of global uneven heating during railway tread braking – Brake rig testing and field study

Article

Institution of MECHANICAL ENGINEERS
Journal of RAIL AND RAPID TRANSIT

Proc IMechE Part F:
J Rail and Rapid Transit
2025, Vol. 0(0) 1–14

DOI: 10.1177/09544097241312943
journals.sagepub.com/home/pif
Sage

Characterisation and evaluation of global uneven heating during railway tread braking – Brake rig testing and field study

Eric Voortman Landström, Tore Vernersson and Roger Lundén

Abstract

In this paper, an effort has been made to characterise and evaluate the risks caused by global uneven heating, which can occur on tread braked railway wheels during prolonged braking. Brake rig experiments and a field study were performed on tread braked railway wheels exposed to brake power levels corresponding to down-hill braking. The brake rig testing was performed at the brake test rig at Chalmers University, with controlled testing at constant power levels of three different types of railway freight wheels. The field experiments were performed on the Ofoten Line outside of Narvik, where the wheel temperatures were measured thermographically. It is found that both the rig testing and the field study may generate a substantially uneven circumferential distribution of the wheel temperatures during tread braking. For the brake rig results an initially even distribution of tread temperatures changes into a state with one concentrated hot zone covering roughly one-fourth to one-third of the wheel circumference. Temperature differences between hot and cold zones on the wheel may then be more than 200°C. Similar behaviour is seen for wheels in the field study at the Ofoten Line, with temperature differences of up to 70°C. Ultrasonic measurements on wheels tested in the brake rig show that the residual stress level in the wheel rim had shifted significantly towards a detrimental tensile state compared to what could be expected from uniform heating. The thermal behaviour is similar for the three wheels that have different web shapes and propensities for the build-up of residual stresses. The global uneven heating is most pronounced at intermediate brake power levels of 25 to 40 kW. The conclusions drawn from the present study are that there can be severe consequences of an assumption of uniform wheel heating with respect to the thermomechanics of the brake–wheel–rail system.

Keywords

Elevated temperature, brake rig testing, field studies, pearlitic steel, railway wheels, tread braking, wheel performance

Date received: 9 July 2024; accepted: 20 December 2024

Introduction

Tread brakes provide a low-cost and maintenance-efficient braking system and are commonly used in both freight and passenger vehicles. However, elevated wheel temperatures occur during prolonged drag braking actions due to the frictional heating.[1,2] Should long-duration brake applications occur, either from braking on long gradients or from system malfunction or flawed driver behaviour, it could result in situations where the mechanical strength of the wheel is jeopardised. Specifically, material plastification occurring at high temperature levels can create significant tensile residual stresses in the wheel rim. This residual stress field is highly dependent on the temperatures achieved during prolonged braking, with higher temperatures normally correlating with larger tensile residual stresses. The thermal and thermomechanical behaviour of the wheel–brake system has been extensively studied previously.[1–11] It has long been known that the contact between the brake shoe and the wheel is characterised by the presence of frictionally induced ThermoElastic Instabilities (TEI) with for example 'hot spots' arising on the wheel tread.[7,8,11–14] This is further complicated since the heating may be unevenly distributed around the wheel circumference as found in previous studies.[15,16] By heating during braking, large global differences in temperatures between a hot and a cold side of a wheel may arise and generate out-of-roundness of the wheel that directly impacts wheel–rail rolling contact forces.

Previous assumptions of evenly distributed heating around the wheel circumference could be valid for small and evenly distributed hot spots, but not for cases with global uneven heating.[16] This is defined as a single period difference in the temperature around the wheel circumference, which could give temperature differences of more than 200°C on the tread. This can lead to material deterioration in hotter zones above some 450°C, since the

CHARMEC/Department of Mechanics and Maritime Sciences, Chalmers University of Technology, Gothenburg, Sweden

Corresponding author:
Eric Voortman Landström, CHARMEC/Department of Mechanics and Maritime Sciences, Chalmers University of Technology, Gothenburg 41296, Sweden.
Email: ericlan@chalmers.se

cementite layers in the pearlitic steel deteriorate into a spheroidised form, with more rapid deterioration occurring at higher temperatures.[17–19] Mechanical characteristics such as yield limit and hardness are lowered as a consequence of this material damage. This then leads to an increase in wear, increased susceptibility to rolling contact fatigue,[20] cracks, spalling and more.

The large temperature differences become increasingly problematic when the entire rail–wheel–brake system is taken into consideration. Trackside wheel temperature detectors are often simple pyrometers, unable to give accurate readings of the maximum wheel temperature of an unevenly heated wheel since only one circumferential point on the wheel is captured. Large variations in the readings can reduce trust in the system and can make wheel temperature warning systems ineffective. Additionally, it is difficult to discover material damage introduced at areas of high temperature as there are indications that the wheel returns to a state of relative roundness after cooling, necessitating metallurgic testing to quantify material damage.

In an effort to investigate the behaviour and effects of global uneven heating, a research campaign has been launched to study the thermomechanical characteristics of the interaction between the tread brake and the wheel. This includes testing in the brake rig at Chalmers University and thermographic field measurements of wheel temperatures of iron ore wagons, owned and operated by the mining company LKAB. The measurements were performed near Narvik on the Ofoten Line, which is the Norwegian part of the Iron Ore Line between the mines in Kiruna in Sweden and the port at Narvik in Norway. Since it is well-known that the design of the wheel web influences the build-up of stresses during braking,[21] and tentatively also the tendency for global uneven heating, three different wheel types are studied in the brake rig.

Experimental testing

The description of the testing is divided into two sections, one for the brake rig tests and one for the field test, as the methodology is different.

Brake rig testing

The laboratory testing is performed using a novel brake rig designed and built within our research centre CHARMEC at Chalmers University of Technology. The power is provided by a 105 kW electrical motor coupled to the wheel axle by a belt drive. This gives a velocity of 60 km/h at the wheel tread when the motor is running at a nominal speed of 1500 rpm. Two BFC tread brake units (4th generation) from Wabtec Faiveley Nordic are mounted on free-swinging arms supported by ball bearings. The arms are constrained in rotation by a force transducer. The brake force given by the tread brake units ranges from 0 kN at 0–0.25 bar to 50 kN at 5 bar pneumatic pressure. One of the two arms is shown in Figure 1a; the other is on the opposite side of the wheel. The brake blocks are mounted in a 2xBg configuration (a single brake block on each side of the wheel). Organic composite brake blocks of K-type are used, of a type having high wear resistance at high temperatures,[22] see the draft version of EN 13979-1.[23] New brake blocks were bedded in for each studied wheel prior to the brake testing.

The tests are performed using constant brake power between 20 kW and 50 kW and a constant speed of 60 km/h. Data acquisition is performed by a National Instruments Compact DAQ device[24] and the brake power is controlled using a measurement programme written in LabView.[25] The temperatures are measured using separate and complementary methods, see Figure 1. Two sliding thermocouples are put into contact with the rotating wheel rim, giving an emissivity-independent measurement of the average temperature over single lines around the wheel tread. However, the thermocouples are unable to resolve the circumferential variation over the tread due to the large time constant.

To determine the temperature variation over the wheel tread and parts of the field side of the wheel rim, a FLIR X6541sc thermographic camera[26] is set up to capture a subwindow of 8 × 320 pixels at 2000-3000 Hz (depending on the temperature measurement interval). At the velocity of 60 km/h, the wheel moves approximately 6-8 mm between each frame, giving roughly 0.75-1 mm/pixel resolution in the circumferential direction. The three tested wheels are coated with high temperature-resistant spray paint to attain a well-defined emissivity over the field side of the wheel. One unpainted metal area is kept on the wheel rim to synchronise the wheel revolutions as the lower thermal radiation can be detected after the data has been processed. A stainless steel mirror reflects the tread when detecting tread temperatures, see Figure 1(a). The mirror has a reflectance of approximately 0.9 for infrared radiation[27] and the remaining error will be contained within the emissivity calibration detailed in the next paragraph. The mirror is periodically dusted to preserve the reflectance. The setup is shown in Figure 1(a) where also thermocouples glued to the wheel web can be seen. The thermographically captured area on the braked wheel is shown in Figure 1(b), which provides results for the wheel tread (in the mirror) and the exterior part of the wheel.

The thermographic temperature values on the tread were calibrated first calculating the average thermographic temperatures and comparing them to the thermocouple temperatures (both in Kelvin), giving an effective emissivity. This correction is then applied to the temperature values on the tread. For disc brakes, a similar method is used in for example[28] This somewhat also reduces the error due to for example dust on the mirror, as it is accounted for in the effective emissivity value. It should be noted that the thermographic measurements are primarily qualitative as the distribution of temperatures is of primary interest, rather than exact temperature values. Thermographic measurements are already a tried-and-tested method used extensively in prior research.[11,29–31]

Several test runs were performed on three different freight wheel designs machined to diameters between 840 and 890 mm (corresponding to wear limit diameters). The chosen wheel designs are characterised by differently shaped wheel webs in which Wheel 1 has an S-shaped web, Wheel 2 is a so-called low-stress wheel with a strong web curvature, and Wheel 3 has a rather straight web with a slight S-shape. The testing procedures for the wheels are

shown in Table 1. Test durations are chosen to limit temperatures and preserve blocks. Wheel 3 had prior to the tests been subjected to revenue service, whereas Wheels 1 and 2 were newly manufactured. This is reflected in the initial residual stress levels in the rim after machining, where a minor difference between the wheels was found. For Wheels 1 and 2, five tests were performed, three tests at 30 kW and then two tests at 50 kW. For Wheel 3 it was realised that a more detailed study on the evolution of the stress field could be of interest, meaning that eleven tests were performed, starting at 20 kW.

The residual stress measurements are performed using an ultrasonic stress measurement device "DEBBIE".[32] For the

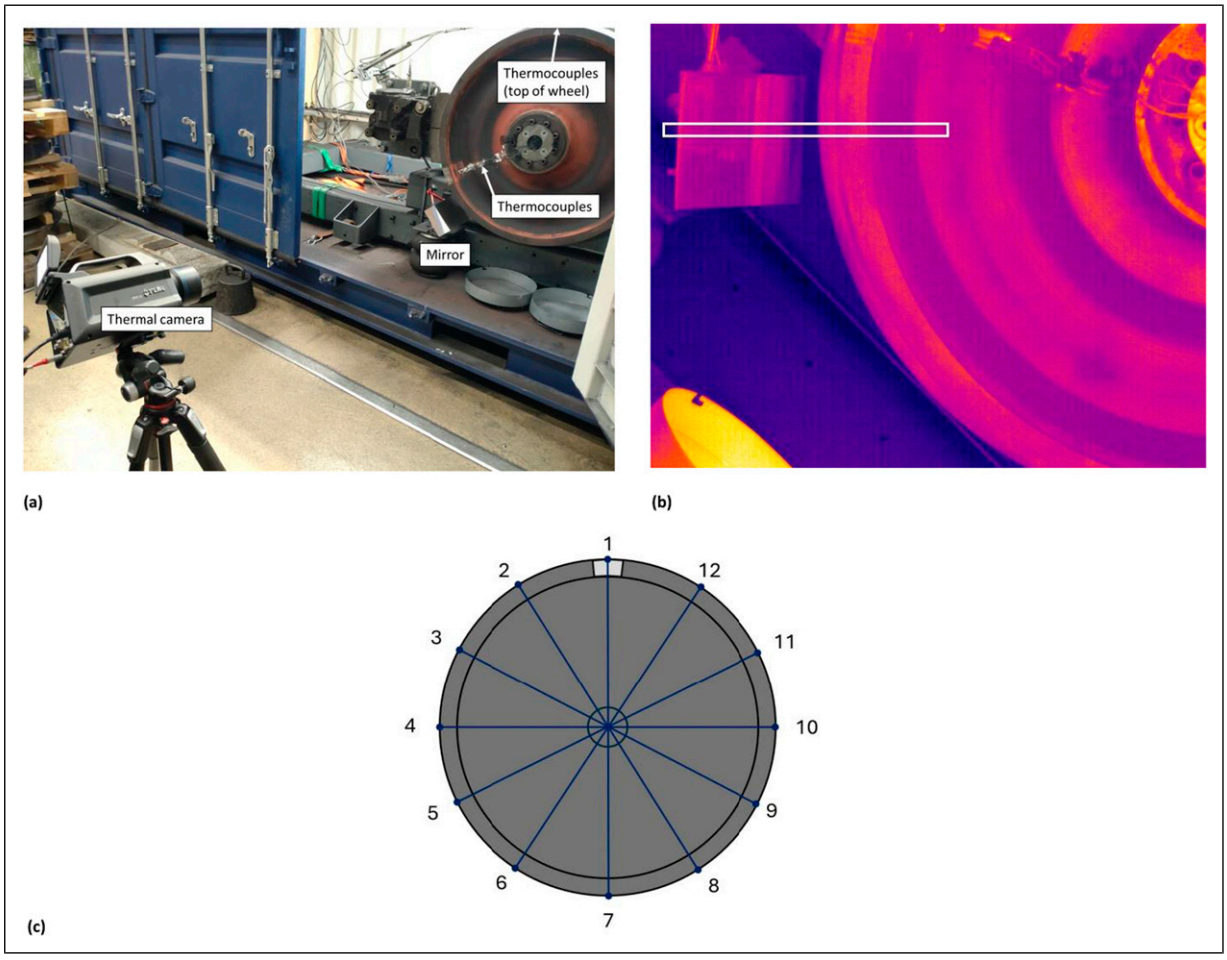

Figure 1. Temperature measurement setup, (a) thermal camera relative to wheel with sliding thermocouples on wheel tread and glued-on thermocouples on wheel web, (b) full camera view with white rectangle indicating approximate pixel area captured during measurements. (c) Positions for the stress measurements. Note that three measurements were taken at each position.

Table 1. Testing programme for the three wheel designs. The first value shows the average brake power (kW) and the second value is the total time (min) of the tests.

	Wheel 1	Wheel 2	Wheel 3
Design	S-shaped wheel	Low-stress wheel	Slightly S-shaped web
Diameter (m)	0.84	0.86	0.89
Test 1	30 / 45	30 / 40	20 / 40
Test 2	30 / 45	30 / 40	20 / 40
Test 3	30 / 45	30 / 40	25 / 40
Test 4	50 / 30	50 / 30	25 / 40
Test 5	50 / 30	50 / 30	30 / 40
Test 6	- / -	- / -	30 / 40
Test 7	- / -	- / -	35 / 40
Test 8	- / -	- / -	35 / 40
Test 9	- / -	- / -	40 / 40
Test 10	- / -	- / -	40 / 40
Test 11	- / -	- / -	50 / 40

first eight tests (all tests on Wheel 1 and the 30 kW tests on Wheel (2) measurements were only made at positions 1, 5 and 9 (see Figure 1(c)), based on the procedure given in the standard EN13979-1.[23] When it was realised that a higher granularity level may be necessary, measurements were taken on all of the twelve points. For each position, stress measurements were taken at three points across the rim thickness. Note that the area around point 1 is shown brighter in Figure 1(c), since it was kept unpainted as mentioned above regarding the thermographic measurements.

Out-of-roundness (OOR) measurements were performed using a mechanical displacement probe and a rotation sensor. The results were collected using a National instruments PCIMIO-16XE-10 and a custom LabView script. OOR was measured before the first test on all wheels and for Wheels 1 and 2 after the final test every 10 mm laterally on the tread. For Wheel 3 it was measured after every test at lateral positions 25, 45 and 65 mm from the field side of the rim.

Field measurements

The thermographic measurements were performed on passing wagons at the closed-down train station in Straumsnes, approximately 13.8 km from the LKAB bulk port in Narvik, and 28.9 km from the Norwegian-Swedish border. The elevation difference is approximately 500 m between the highest altitude near the border and Straumsnes. The gradient is shown in Figure 2(a). The iron ore trains have axle loads of 31.5 tonnes, resulting in applied brake power levels as calculated in Figure 2(b), presuming a train speed of 50 km/h and no electrodynamic braking of the locomotive. In practice, the brake power is rather constant as the driver does not adjust the braking force for short intervals of lower gradient as the re-application time can be noticeable. The thermal inertia will also prevent significant cooling and evening-out of the temperature field during any short breaks in the brake applications.

Thermographic measurements on the passing freight train wheels were made using the same FLIR X6541sc thermographic camera. However, in these tests the camera was used in full window mode, capturing the passing train wheels with a resolution of 640 × 512 pixels at 40–50 Hz. The camera was placed on the platform, roughly 8 m from the second track which the loaded trains bound for Narvik use. The setup is shown in Figures 2(c) and 2(d).

The analyses of the wheels are performed by image recognition using the circular Hough Transform as implemented in the function *imfindcircles* in MATLAB. The images are binarized using a limit of 100°C (lowest temperature for the used calibration range) and wheels are then identified, see Figure 3 where a comparison is made. Some cold wheels are not identified by the detection algorithm as they are not visible in the binary images, though these wheels are presumed to not show measurable levels of global uneven heating, see Figure 12.

Mean temperatures are determined by estimating the wheel rim position from the images and then averaging the temperature over all of those pixels. This provides a robust measurement because of the large number of pixels. The variation in rim temperatures is determined by calculating the average temperature along several different radial lines crossing the wheel rim, repeated for all images of the same wheel. If there is a consistent variation in temperature, the wheel is considered to be suffering from global uneven heating.

Brake rig testing results

The results are presented in two sections, one for Wheels 1 and 2 and one for Wheel 3. This is because the testing methodology is different as noted in Chapter 2.

Wheels 1 and 2

Sliding thermocouple data for the tests on Wheels 1 and 2 are shown in Figure 4. These were established by taking the maximum temperature of the two thermocouples at each time step as the lateral sliding motion can cause temporary drops in temperature. Using maximum values gives a relatively stable and repeatable representation of tread temperatures.

Thermographic measurements of the wheel tread temperatures after 20, 30 and 40 minutes of testing are shown in Figure 5. Because of the large differences in actual temperatures during the tests, all values are given as thermographic temperature relative to the maximum thermocouple measurement (in Kelvin) for each test. No global uneven heating is visible during the first 30 kW test, until after some 40 minutes when a minor hot zone forms between points 9 and 12 in Figure 5. Global uneven heating however visible for both wheels shown during tests 2–5. Moreover, it is evident that although the hotter areas are not necessarily stationary on the wheel between tests, they are approximately stationary during each test, with a slow migration occurring. This means that approximately one-third to one-half of the wheel is being subjected to significantly higher temperatures when compared to average thermocouple temperatures in Figures 4(a) and 4(b).

Comparing high temperature zones with measured high tensile residual stresses shown in Figure 6, some correlation is observed. Regarding Wheel 1, the stress is almost constant after the first two tests despite a local elevation of temperatures around points 1 and 12. However, a large peak can be seen at point 9 after the third test, correlating to the high temperatures around point 8, see Figure 5. The large increase in stress around points 7-10 for test 3 also directly relates to a localised hotter region. For tests 4 and 5 at the higher power level of 50 kW, no clear correlation can be seen. For Wheel 2, the only stress measurement that would relate to thermal localisation would be after test 3, where the highest measured stress is found at position 5. This corresponds to the approximate centre of the hot temperature zone seen in Figure 5(b), 5(d) and 5(f). Results of (mean value-subtracted) measurements of wheel tread out-of-roundness (OOR) are shown in Figure 7. The measurements were here performed prior to test 1 and after test 5, meaning it is not possible to determine change per test. It is evident that OOR significantly increases after the testing,

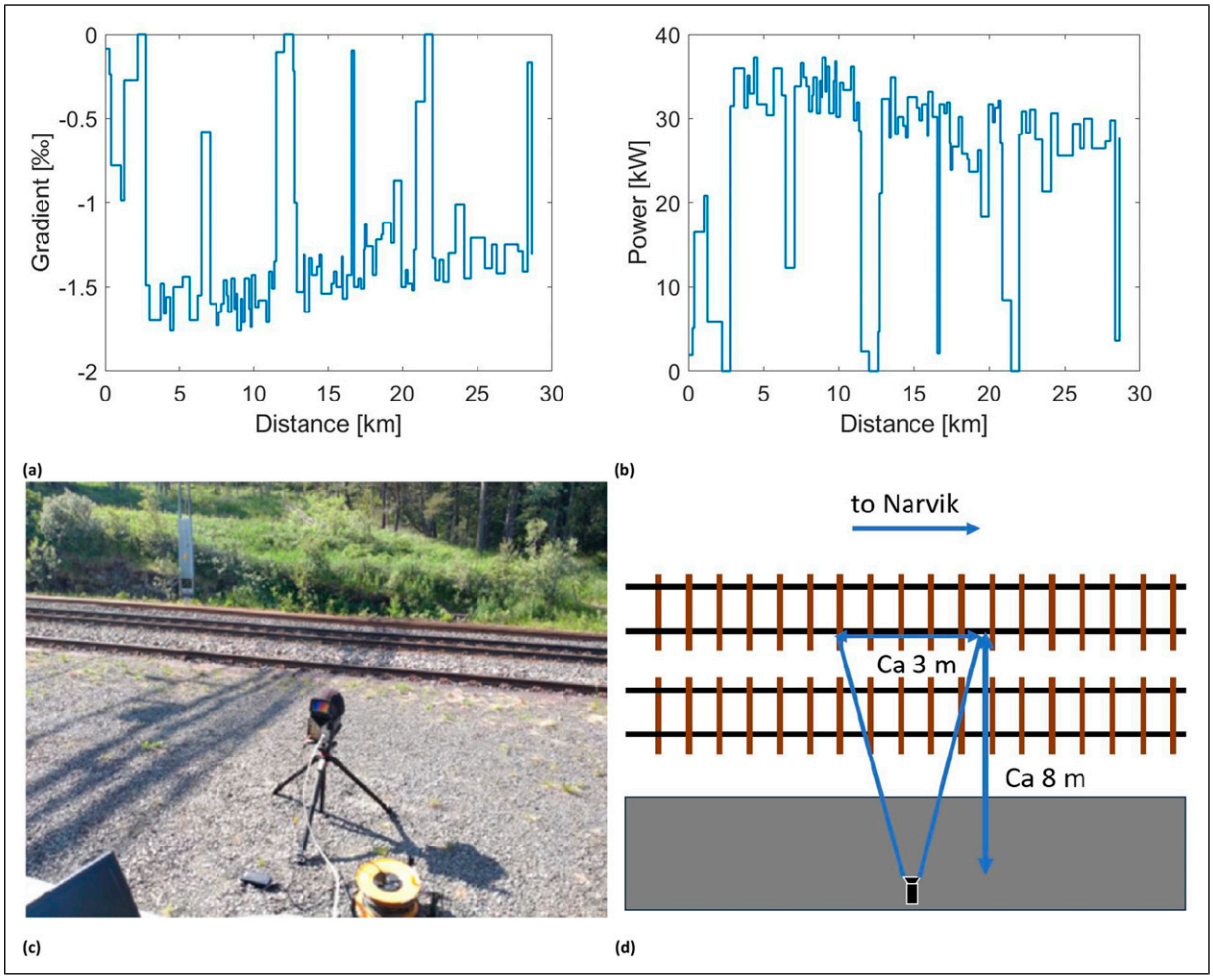

Figure 2. (a) Gradient (‰) and (b) calculated brake power (kW) per wheel for the freight trains between the Norwegian–Swedish border and Straumsnes near Narvik. (c) Thermographic camera setup in Straumsnes. (d) Drawing of the approximate position of the camera relative to the descending rail (furthest from the camera).

with the range (valley to peak value) rising from about 0.10 mm prior to testing to 0.21 mm and 0.26 mm for Wheels 1 and 2 respectively after tests. Initial OOR can influence global uneven heating for the first two brake cycles on Wheel 1 and the first three on Wheel 2, for which the highest (most protruding) areas correspond to the highest temperatures and vice versa. Regarding final OOR and temperatures at testing, it is difficult to find a clear trend. Tentatively, for Wheel 1, temperatures of the last brake cycles and final OOR could be related in similar ways as the initial ones, with high peaks corresponding to high temperatures, whereas for Wheel 2 it seems as if areas with high temperatures correspond to valleys in OOR.

Wheel 3

It was determined to investigate global uneven heating for lower brake power levels and to improve the fidelity by including testing at more power levels between 20 and 50 kW. Power 20 kW corresponds to braking on a 6.5‰ gradient at speed 100 km/h and axle load 22.5 tons. Temperatures as measured by the two sliding thermocouples are shown in Figure 8. As noted for the previous thermocouple results, only the maximum value for the two thermocouples is shown. The curves are all reasonable and show similar behaviour between the tests at every level.

The residual circumferential stress field as measured by the ultrasonic probing at the 12 measurement points is shown in Figure 9, with the measured values and the stress range over the circumference being presented. Of significance here is the variation seen in the initial field, with an almost 60 MPa difference over a distance corresponding to half the wheel circumference. This tendency continues through the first four tests, with a sharp decrease after test 5 (first test at 30 kW) until it increases again after test 11 (first and only test at 50 kW). One detail to note here is that the residual stress field stays almost constant for successive brakings at the same power level, except for test 6 which shows a noticeable increase. This may be related to non-uniform heating as will be discussed later in this section.

The thermographic temperatures are shown for each power level as measured during one revolution at 20, 30 and 40 min after start, using the same calibration procedure for emissivity as the previous two wheels. Compared to the average thermocouple temperatures shown in Figure 8, the maximum thermographic temperatures tend to be significantly higher due to the hot spots that form, which the slower-reacting thermocouples cannot register. It should be

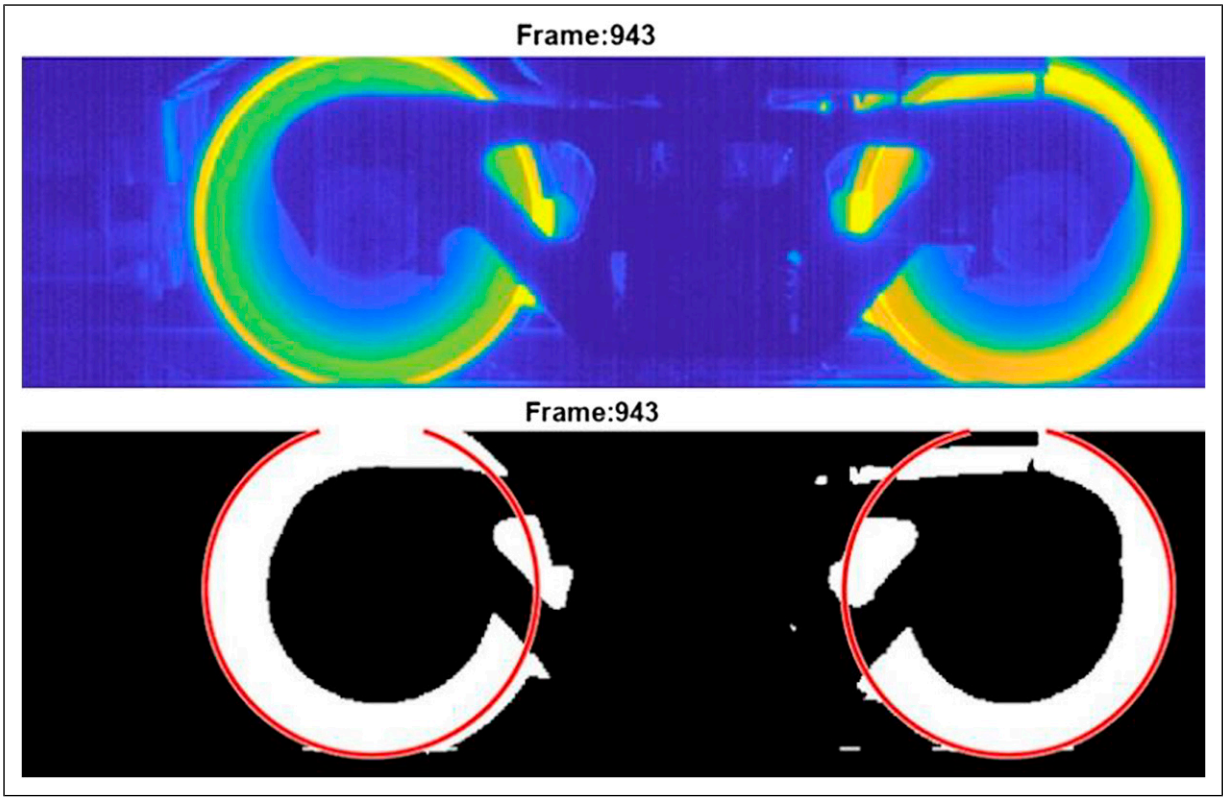

Figure 3. (above) Example of a thermographic image of a wheel, (below) binarized image with the identified wheel circles shown in red. Note that the identified circles intentionally do not cover all the white parts of the image, some of which is the brake block and some of which is the wheel tread (left wheel, right side). Also, note that the bogie frame covers part of the wheel, but this does not impact the analysis.

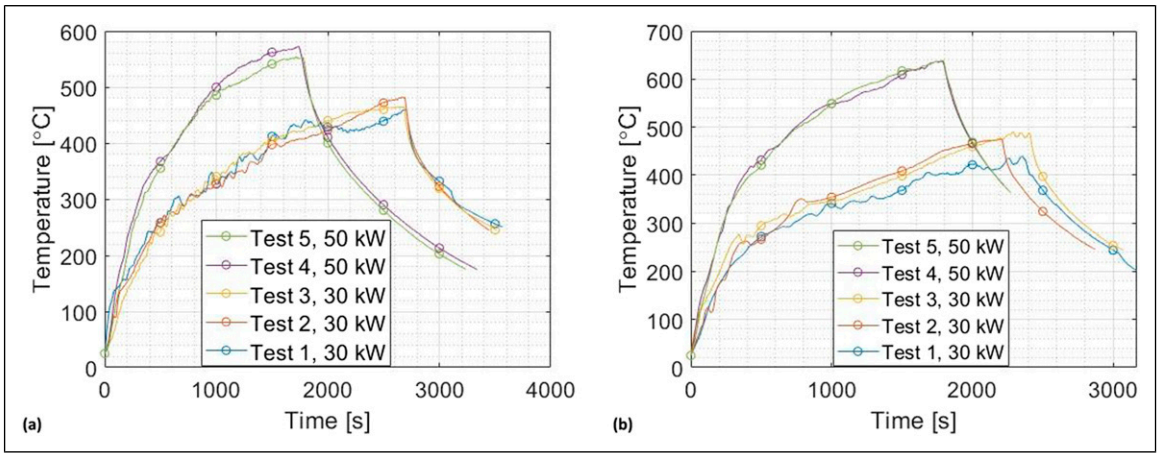

Figure 4. Average temperatures as measured by sliding thermocouples. (a) Wheel 1, tests 1 to 5, (b) Wheel 2, tests 1 to 5. Note that the temperatures shown are the maximum of the two thermocouples at each time step as they can vary noticeably due to sliding in the axial direction.

noted that the mirror for the thermographic camera may have been somewhat out of alignment to capture the entire wheel tread width during some of these tests, meaning that the tread away from the flange is not entirely captured. Nevertheless, a heat flux variation laterally (i.e. left-right in the images of the tread) with respect to the centreline of the tread can often be identified, see for example the final tests at 50 kW where the highest temperatures form a slight 'S'-shape. By studying the field side of the rim, to the right of dotted lines, it is found that high temperatures on the rim front face correspond to high temperatures near the field side of the tread in correspondence with the 'S'-shape. It can moreover be noted that denser clusters of hot spots form on the tread, which causes some localisation. The second test at 30 kW, presented in Figure 10(a), 10(c) and 10(e), shows that laterally unevenly distributed heating on the tread, with the heat tending towards the field side on one half of the wheel and towards the flange on the other half.

Finally, wheel out-of-roundness measurements for the three positions (25, 45 and 65 mm from the field side of the

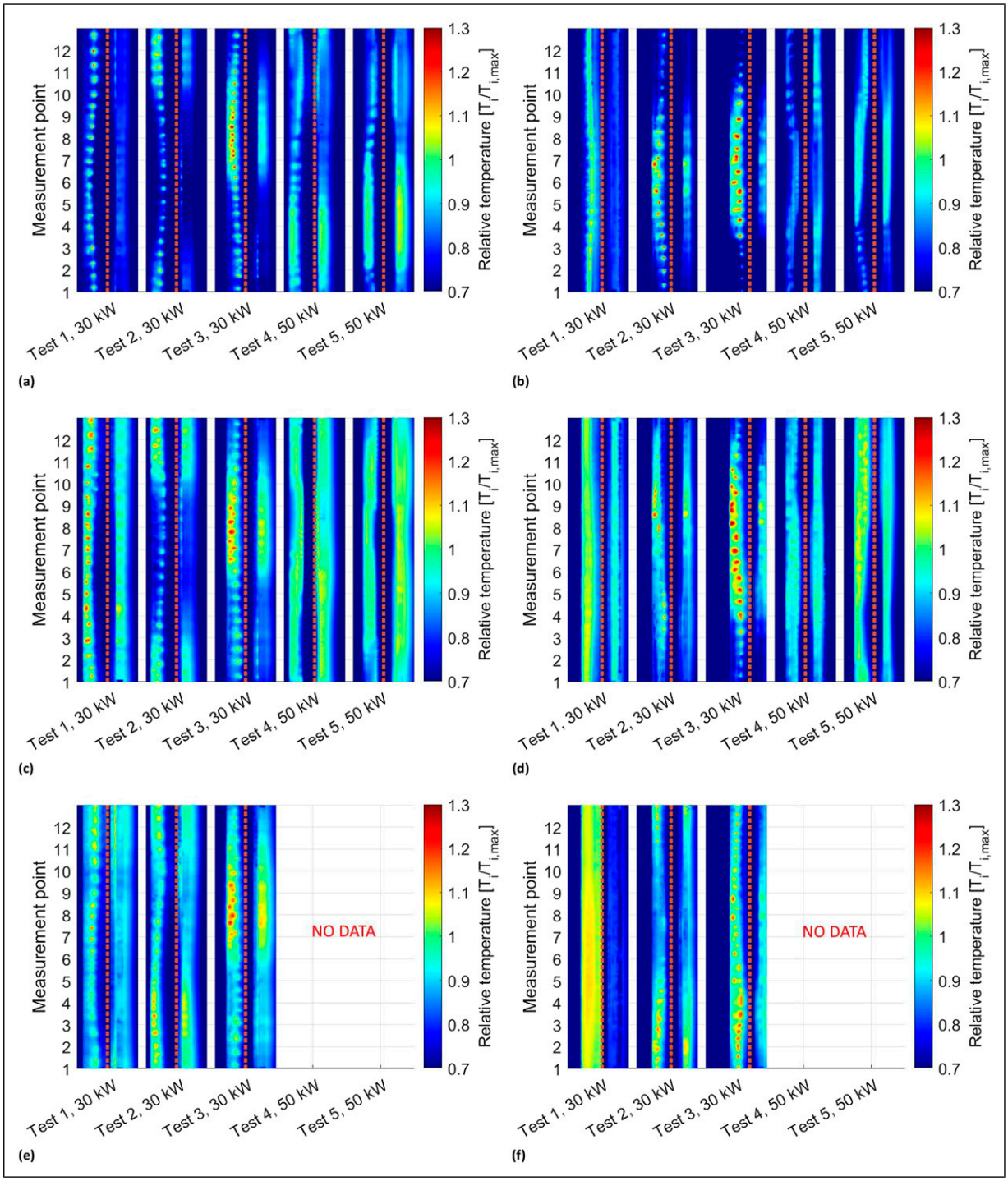

Figure 5. Thermographic images of wheel tread and rim front face, see Figure 1(b), during one revolution for different tests at the selected time after test start for Wheels 1 and 2. Positions where residual stresses were measured, see Figure 1(c), are indicated on vertical axes. Dotted vertical lines separate the wheel tread on the left from the rim front face and web on the right, c. f. Camera view in Figure 1(b) (a) Wheel 1, 20 min, (b) Wheel 2, 20 min (c) Wheel 1, 30 min (d) Wheel 2, 30 min, (e) Wheel 1, 40 min, (f) Wheel 2, 40 min. Note that the white bar separates different tests. Also, note that no data are shown for the 50 kW tests at 40 min because the tests had been terminated. Values are normalised in Kelvin.

rim) are presented in Figure 11 for the initial wheel circumferences as well as after each of the 11 tests. The average values have been subtracted to give the out-of-roundness values to give prominence rather than absolute measurements. It should be noted that there are no guarantees that the out-of-roundness behaves similarly during the heating process, in particular, due to increased wear on protruding surfaces. This may contribute somewhat to the evening out of the OOR during the latter half of the tests. It can be seen from the initial measurements in Figure 11 that the initial OOR range is approximately 0.02 mm and that it correlates well with the induced temperatures on the tread, with the highest temperatures forming in areas that have the largest protrusions. A single period OOR prevails for the initial tests, being roughly constant in shape and with a range below 0.10 mm, until after test 7. For the tests at even

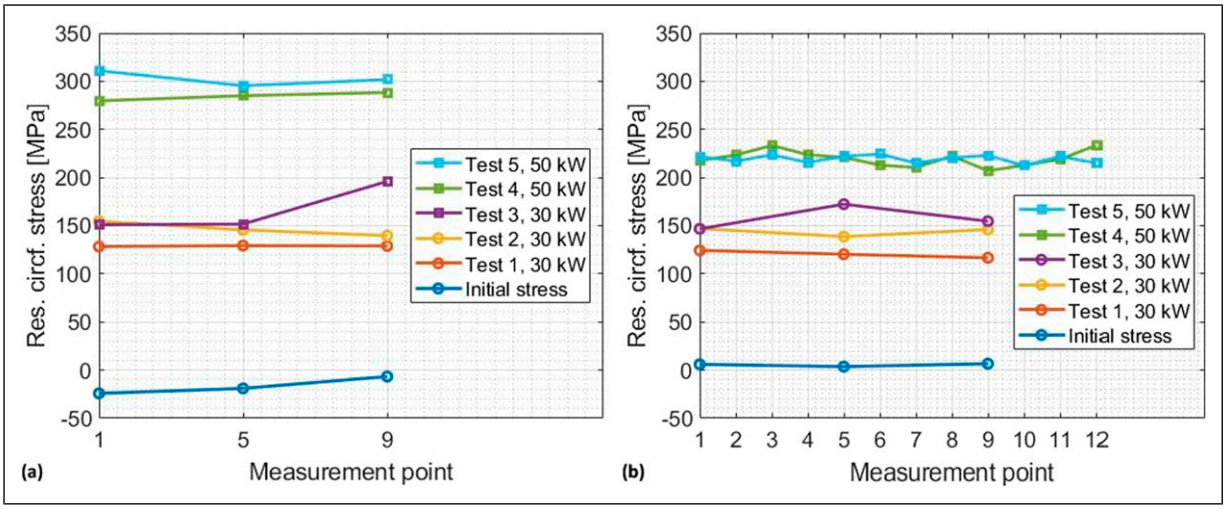

Figure 6. Measured average residual circumferential stress values before tests and after selected tests. Averages plotted against measurement point (see Figure 1(c)) for (a) Wheel 1 and (b) Wheel 2

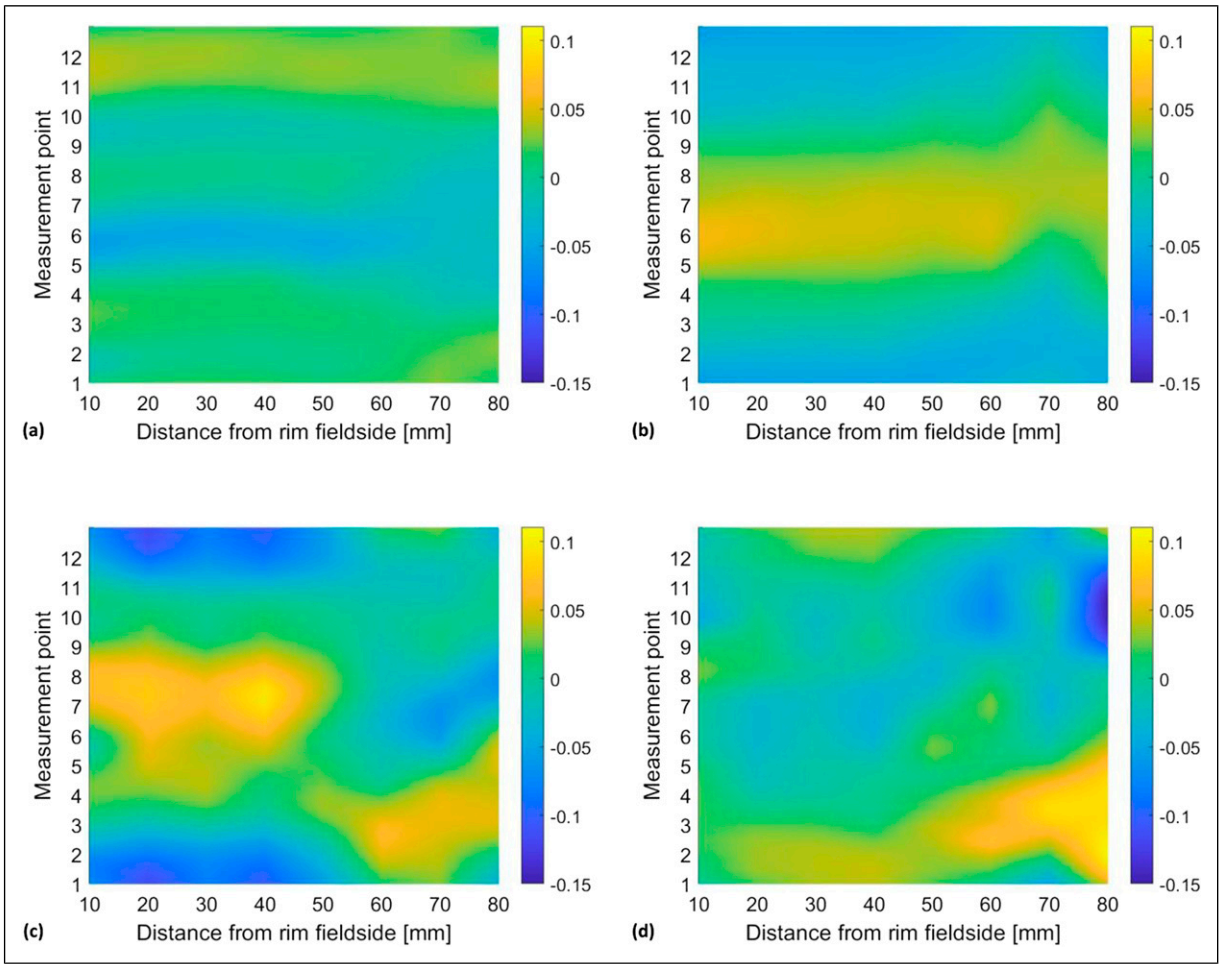

Figure 7. OOR values measured by contact probe over wheel tread width for one revolution indicated by stress measurement positions 1–12. (a) OOR values before testing for Wheel 1, (b) OOR values before testing for Wheel 2, (c) OOR values after testing for Wheel 1, (d) OOR values after testing for Wheel 2.

higher power levels, the OOR shows a slow phase change in that the peak switches from (approximately) position 11 to position 4, corresponding to the diametrically opposing side. It also increases in magnitude, from 0.10 mm to 0.14 mm.

Studying all of these measurements in conjunction, a few details emerge. The thermographic fields in Figure 10(a), 10(c) and 10(e) show a tendency of higher temperatures/ laterally shifting towards the field side at measurement points 9 to 12.

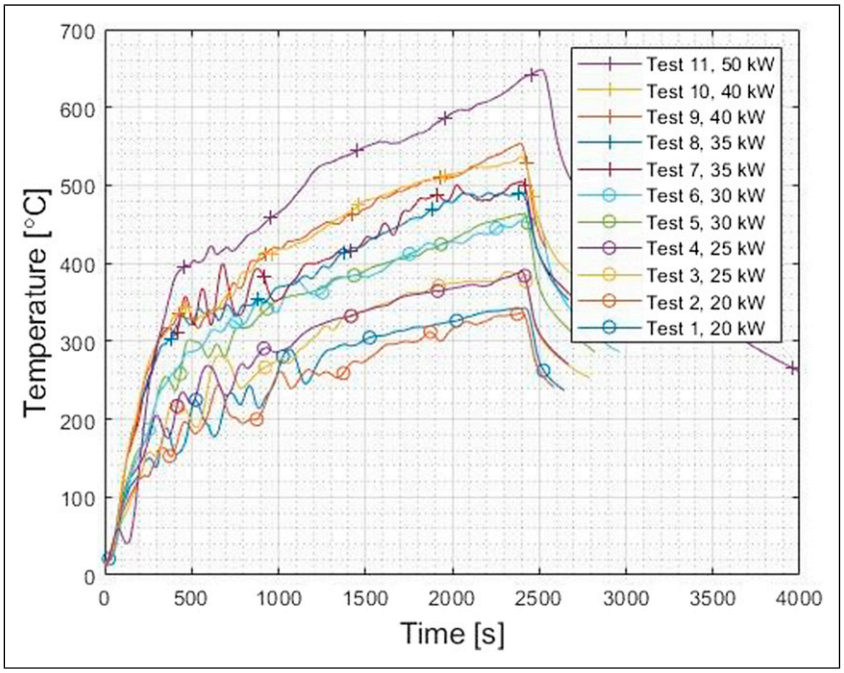

Figure 8. Thermocouple temperatures as measured during all 11 tests of Wheel 3. Note that the temperatures shown are the maximum of the two thermocouples at each time step.

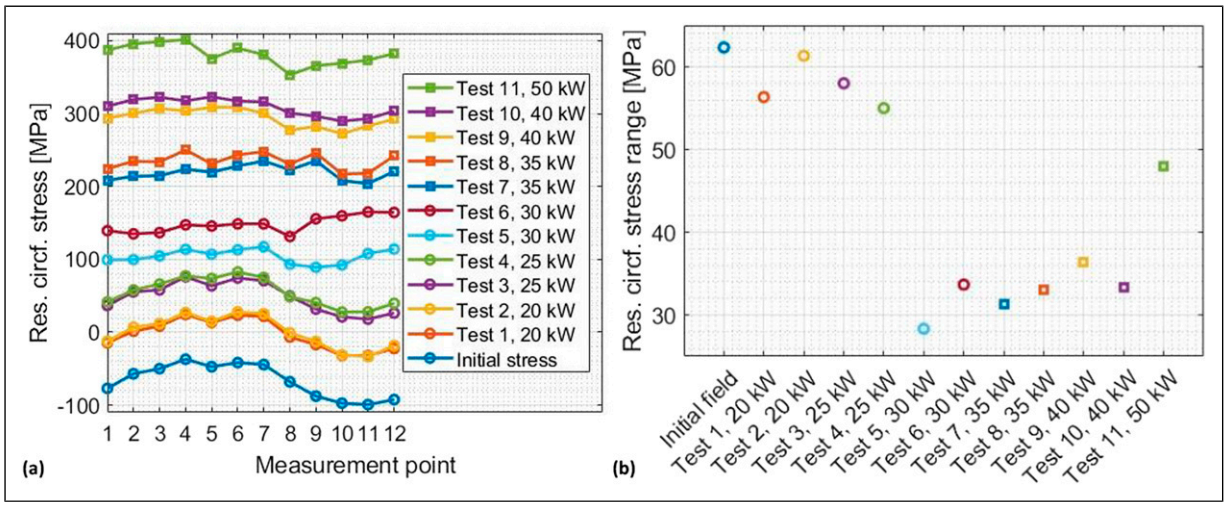

Figure 9. Measured average residual circumferential stresses. (a) Averages plotted against measurement point (see Figure 1(c)) for all tests including initial values, (b) total range (max-min) after each test.

This can be compared to the OOR measurements in Figure 11, which show a peak around the same points. The stress field variation is however unaffected by this, with only the mean stress level increasing until after test 5, as noted before. Comparing this to the temperatures, one can note that there is an area with notably higher temperatures around point 11. After this test, the stress levels are more uniform until the final test at 50 kW. One might also consider that the temperatures from test 7 and onwards are relatively evenly distributed, showing more of a lateral shift on the tread rather than one singular concentration. This is potentially reflected in both the stress measurements and the OOR measurements being somewhat more evenly distributed, until the final test where the OOR spikes. This evident increase in OOR occurs in the same range as the highest stress values for that test in addition to the stress range increasing, but there are no indications that this is due to a thermal localisation. This repeats the results from the first two wheels in that it is difficult to find a clear tendency whether the non-uniform temperatures negatively affect the residual stress field.

Field tests results

Only thermographic results from the wheel field sides are available from the field measurements. Because only thermographic data is available, no calibration comparable to the lab. one can be made, so any temperature value comparison is qualitative.

In total, thermographic data on wheel temperatures were acquired for 14 LKAB iron ore freight trains

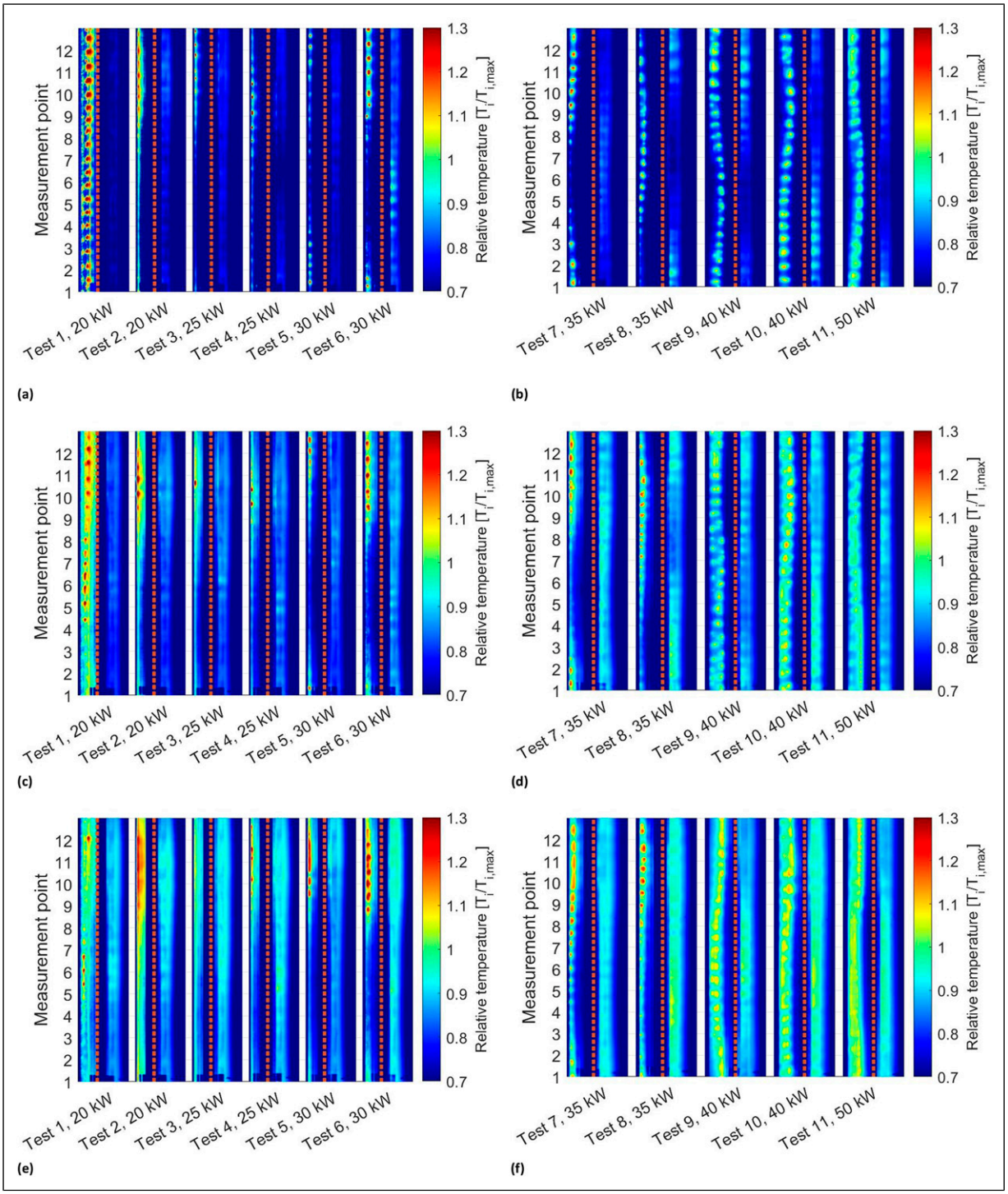

Figure 10. Thermographic images of wheel tread and rim front face during one revolution for different tests at the selected time after test start for Wheel 3. Positions where residual stresses were measured, see Figure 1(c), are indicated on vertical axes. Dotted vertical lines separate the wheel tread on the left from the rim front face and web on the right, c. f. Camera view in Figure 1(a) and (b) Tests at 20–30 kW, 20 min, (b) tests at 35–50 kW, 20 min, (c) tests at 20–30 kW, 30 min, (d) tests at 35–50 kW, 30 min, (e) tests at 20–30 kW, 40 min, (f) tests at 35–50 kW, 40 min. Note that the white bar separates different tests. Values are normalised in Kelvin.

during 3 days of measurements, the total being approximately 3800 wheels. The distribution of mean temperature for the distinguishable wheels (roughly 350 out of 3800 were below the detection limit of 100°C) is shown in Figure 12a. The large variations in wheel mean temperatures can largely be attributed to (1) some loaded trains had to wait for meeting trains at siding (allowing the wheels to cool), (2) variations in utilisation of electrodynamic braking by train drivers, (3) differences in wheel designs and wheel diameters, and (4) differences in braking efficiency for different wagons and also in bogies. The mean temperatures for the hottest wheels are similar to those from brake rig testing at 20–25 kW.

Moreover, the thermographic data corroborated that tread braked wheels in field conditions exhibit global uneven heating, see example in Figure 12(d). However, on average, only a few wheels per train are affected, and

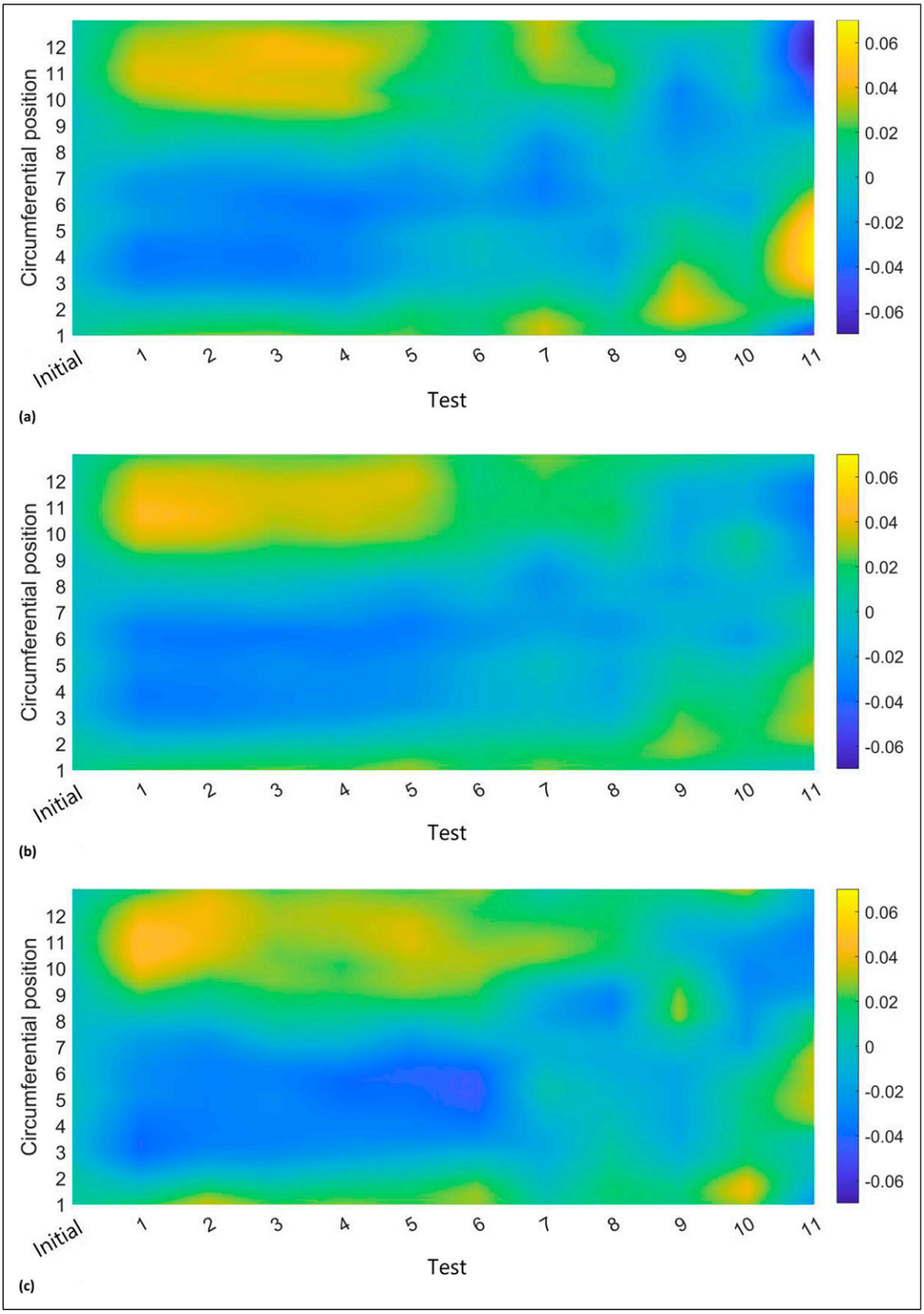

Figure 11. OOR measured by contact probe over one revolution after all tests including initial values, at distance from field side of rim (a) 25 mm (b) 45 mm, and (c) 65 mm.

the temperature variations are below 80°C, see Figure 12(c). These values can be compared to the rim values of the previous thermographic results for the most comparable tests (i.e. 30 kW and below), which show differences of perhaps 0.1-0.15 $T_{i,max}$, or 60 to 90°C (noting that the maximum value is normalised in Kelvin). The field measurements are expected to show generally lower results due to the lower effective emissivity, rail chill effect and possibly better convection, but the values are nonetheless comparable.

The low number of wheels with localisations above 30°C (9 wheels) when compared to the total number of wheels (Figure 12(a)) shows that this is not a critical issue on the Ofoten Line as of today. However, when considering wheels with an average temperature higher than 200°C it is found that 8% exhibit global uneven heating and for wheels hotter than 220°C it has increased to 15%. This implies that the phenomenon becomes more frequent with increasing braking power. The overall low frequency of global uneven heating for the wheels on the Ofoten Line is thus aided by

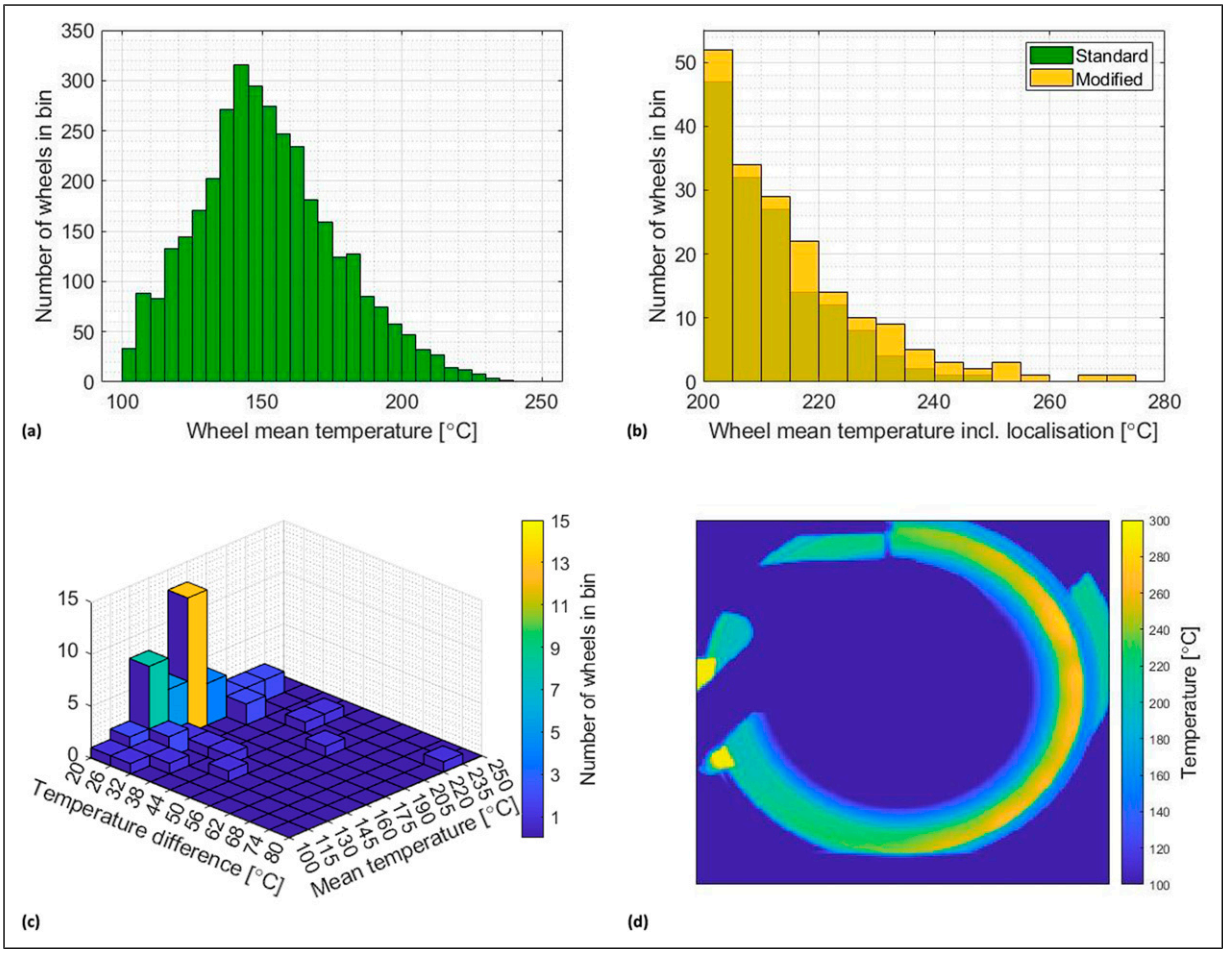

Figure 12. (a) Distribution of mean temperatures of wheels. (b) Temperature distribution of the hottest wheels, with standard distribution based on wheel mean rim temperature (as in Figure 12a) and with a modified distribution that accounts for maximum temperature for wheels with global uneven heating. (c) Distribution of temperature difference of wheels with global uneven heating above 20°C on the wheels. (d) Example of a wheel showing strong global uneven heating with temperature in C. Note bogie frame shrouds the wheel on the left.

the fact that the line is fully electrified with efficient electrodynamic braking, leading to relatively low brake power levels.

The thermographic data also facilitates a detailed analysis of the distribution of wheel temperatures. In Figure 12, the distribution of the wheel mean temperatures is shown in green (i.e. same results as in Figure 12(a)) and the temperature distribution accounting for thermal localisation is overlaid in yellow. As can be seen, this leads to a substantial increase in the number of hot wheels. These would then suffer more material damage than expected due to large volumes with elevated temperatures.

Discussion and conclusion

First and foremost of the results shown is the tendency of the temperature field on the wheel tread to localise during braking, especially at brake rig testing but also at field conditions. This would suggest that the phenomenon is (at least partially) independent of the rail chill effect or the superior cooling conditions in field, although rail chill does impact the severity of the non-uniformity. Rail chill is estimated via the methods in[1] to remove approximately one third of the heat or 10 kW, with a variation of ±10% for the hotter and colder wheel sectors respectively. This can be compared to the 5 kW that is estimated to be required to heat a wheel at 240°C an additional 40°C, comparable to the largest non-uniformity seen. Rail chill may thus account for a cooling of perhaps 20°C of the hottest sector.

As seen in Figures 5 and 10, all three wheels exhibit global uneven heating for all tests bar the first one, either by a circumferentially varying temperature or by a laterally varying temperature (forming an S-shape on tread). The patterns of uneven temperatures are mostly stationary for each test and also between tests at lower braking power levels. However, when braking at power levels above 30 kW large variations are seen between tests. Global uneven temperatures of the observed magnitude are expected to significantly accelerate material deterioration, c. f.,[17–19] as the lamellar pearlite breaks down into a spheroidised pearlite. The phenomenon of global uneven heating is likely not directly related to specific wheel designs, as the three investigated types of wheels behave similarly. However, the wheel design can be seen to influence the distribution of temperatures on the treads, in which the wheel with the least flexible wheel web (Wheel (3) seems to have a stronger propensity for laterally shifting heat on the tread (the identified S-shape) and the wheel with the most flexible wheel web (Wheel (2) is less prone to such lateral shifting

temperatures. More testing is required to confirm this conclusion.

The arms to which brake actuators are mounted in the brake test rig are very stiff whereas on a wagon, depending on the brake design and bogie suspension, the brake–wheel interaction may be more compliant. The fact that single period out-of-roundness has been found to form in wheels during braking is likely due to variations in the brake normal force and the contact pressure between the block and the wheel. This results in a local increase of the heat flux on the tread, probably influenced by initial wheel OOR. This implies a feedback loop giving increased contact pressure that further increases the heating. The results also indicate that the wheel design can influence the range of OOR resulting after braking, whereas the wheel with the least flexible web.

(Wheel 3 with a slight S-shape) exhibits the lowest OOR range and the wheel with the most flexible web (Wheel 2 being of low-stress design) has the largest range. Further investigations into brake mounting will be made.

There is some evidence of a relationship between global uneven heating and increased residual stress. Some indications are seen for all wheels when the stress and temperature measurements are compared, but not enough for solid conclusions. In the absence of rail contact, hot spots and global uneven temperatures are seen to be quasi-stationary during a test. For higher power levels, it is suspected that global uneven heating can be alleviated by the combined effect of an increased braking force and an increased flexibility of the brake block material at high temperatures. Overall, a more even contact pressure and tread temperature distribution is then attained, inducing global high levels of residual stress, but with smaller variations. If there is a relationship, locally increased residual stress would have consequences for fatigue and fracture characteristics of the wheel, especially if the hotter and more deteriorated parts of the wheel are repeatedly affected by heating that remains fixed between braking events. Further studies are likely required to determine the effects.

For the field measurements, it is shown that global uneven heating occurs on train wheels although only on a limited amount. The overall temperature differences because of the uneven heating were low compared to the highest ones seen in the brake test rig, although the mean wheel temperatures were also lower. It is shown that hotter wheels are more prone to global uneven heating. Estimations of wheel temperatures using FEM (not shown in the present paper) show that zero to low levels of electrodynamic braking is a reasonable assumption when compared to the measurements for the trains with the hottest wheels.

Regarding the measured wheel temperatures on the Often Line, it is likely that global uneven heating is more of a long-term issue for the entire fleet of wagons regarding wheel life, rather than being the cause of catastrophic events. Future requirements for increased braking power may impact the frequency and magnitude of localised wheels given that increased temperatures, even if localised, can adversely affect wheel integrity. Another issue is the prevention of damage pertaining to global uneven heating. Current detectors measure at one circumferential position only and are thus unlikely to detect the highest temperatures of wheels having global uneven heating with any regularity. Varying temperatures from different detectors may be considered measurement noise rather than early warnings of high wheel temperatures. The relatively quick thermal conduction also means that uneven temperatures tend to disappear rapidly if heating is discontinued, making it difficult to study after braking. It may thus be worth considering novel solutions capable of detecting uneven wheel heating.

Future work is foreseen to continue studying this phenomenon as it is by all accounts a normal effect of brake testing. This will hopefully shed further light on both the causes and the effects of non-uniform temperatures in train wheels. In particular, both the brake rigging stiffness and the rail interaction will be studied with the addition of new modules on the here employed brake testing rig. Additionally, simplified numerical models of the wheel-brake contact interactions are also on the horizon, where the out-of-roundness effects could be studied in more detail.

Acknowledgements

This work is part of the activities within the Swedish National Centre of Excellence CHARMEC (Chalmers Railway Mechanics). The authors would like to express their gratitude to Lucchini Sweden and Lucchini RS in Italy for providing the railway wheels and parts of the brake rig, to Faiveley Transport Nordic for providing the brake actuators and to Becorit GmBH for providing the brake blocks. Mr Jan Moller at Chalmers contributed to the work on the brake rig. Mr Robert Pallari and LKAB and also Mr Thor Braekkan and Jens Harry Hoff and Bane NOR provided support and sponsorship for the field measurements.

Authors contribution

Conceptualization: T.V., R.L., E.L., Methodology: T.V., E.L., Software: E.L., Validation: E.L., T.V., Formal Analysis: E.L., T.V., Investigation: E.L., T.V., Resources: T.V., R.L., E.L., Data Curation: E.L., Writing - Original Draft: E.L., Writing - Review & Editing: T.V., R.L., E.L., Visualization: E.L., T.V., Supervision: T.V., R.L., Project administration: T.V., R.L., Funding Acquisition: T.V., R.L.

Declaration of conflicting interests

The author(s) declared no potential conflicts of interest with respect to the research, authorship, and/or publication of this article.

Funding

The author(s) disclosed receipt of the following financial support for the research, authorship, and/or publication of this article: This study is supported by This work is part of the activities within the Swedish National. Centre of Excellence CHARMEC (Chalmers Railway Mechanics). The field study in Narvik was sponsored by LKAB and Bane NOR. The sponsors did not influence the design of the study, the collection, analysis and interpretation of data, the writing of the report nor in the decision to submit the article for publication.

ORCID iD

Eric Voortman Landström https://orcid.org/0000-0003-0324-2673

References

1. Vernersson T and Lundén R. Temperatures at railway tread braking. Part 3: wheel and block temperatures and the influence of rail chill. *IMechE: Journal of Rail and Rapid Transit* 2007; 221(4): 443–454.
2. Teimourimanesh S, Lundén R and Vernersson T. *Braking capacity of railways wheels - state-of-the-art survey*. In: Proceedings 16th International Wheelset Congress, Cape Town, South Africa, March 14-19, 2010.
3. Parker RC and Marshall PR. The measurement oaf the temperature of sliding surfaces, with particular reference to railway brake blocks. *Proc Inst Mech Eng* 1948; 158: 209–229.
4. Vernersson T. Tread braking of railway wheels noise-related tread roughness and dimensioning wheel temperatures: field tests, rig measurements and numerical simulations. *Chalmers Applied Mechanics*. Gothenburg, Sweden: Doctoral Dissertation, 2006.
5. Vernersson T. Temperatures at railway tread braking. Part 1: modelling. *Journal of Rail and Rapid Transit* 2007; 221(2): 167–182.
6. Vernersson T. Temperatures at railway tread braking. Part 2: calibration and numerical examples. *IMechE: Journal of Rail and Rapid Transit* 2007; 221(4): 429–441.
7. Dufrénoy P and Brunel JF. Thermal localizations in friction´ brakes. 26th Brake colloquium and exhibition, San Antonio, TX, USA, October 12-15, 2008.
8. Dufrénoy P and Weichert D. A thermomechanical model for the analysis of disc brake fracture mechanics. *J Therm Stresses* 2003; 26(8): 815–828.
9. Teimourimanesh S, Vernersson T and Lundén R. Modelling of temperatures during railway tread braking: influence of contact conditions and rail cooling effect. *Proc Inst Mech Eng F J Rail Rapid Transit* 2014; 228(1): 93–109.
10. Teimourimanesh S, Vernersson T and Lundén R. Thermal capacity of tread-braked railway wheels. Part 2: applications. *IMechE: Journal of Rail and Rapid Transit* 2016; 230(3): 798–812.
11. Thuresson D. *Thermomechanics of block brakes, Doctoral Dissertation*. Gothenburg, Sweden: Chalmers Applied Mechanics, 2006.
12. Fec MC and Sehitoglu H. Thermal-mechanical damage in railroad wheels due to hot spotting. *Wear* 1985; 102(1): 31–42.
13. Barber JR, Beamond TW, Waring JR, et al. Implications of thermoelastic instability for the design of brakes. *J Tribol* 1985; 107: 206–210.
14. Yeo T and Barber JR. Finite element analysis of thermoelastic contact stability. *J Appl Mech* 1994; 61: 919–922.
15. Cookson J, Mutton P, Tran L, et al. Tread damage due to extreme thermal localization under high braking loads in heavy haul operations. In: Proceedings 20th International Wheelset Congress, Chicago, IL, USA, May 8-11, 2023.
16. Landström EV, Vernersson T and Lundén R. Analysis and testing of tread braked railway wheel — effects of hot spots on wheel performance. *Int J Fatig* 2024; 180: 108116.
17. Nikas D, Ahlström J and Malakizadi A. Mechanical properties and fatigue behaviour of railway wheel steels as influenced by mechanical and thermal loadings. *Wear* 2016; 366-367: 407–415.
18. Landström EV, Steyn E, Ahlström J, et al. Thermomechanical testing and modelling of railway wheel steel. *Int J Fatig* 2023; 168: 107373.
19. Steyn E and Ahlström J. Thermo-mechanical response of near-pearlitic steel heated under restriction of thermal expansion. *J Mater Res Technol* 2024; 32: 1714–1724.
20. Kato T, Kato H and Makino T. Effect of elevated temperature on shelling property of railway wheel steel. *Wear* 2016; 366-367: 359–367, Contact Mechanics and Wear of Rail / Wheel Systems, CM2015, 2015.
21. Ali E, Vernersson T, Nikas D, et al. High temperature tread braking simulations employing advanced modelling of wheel materials. In: Proceedings International Heavy Haul Association Conference. Sydney, Australia, 21-24 June 2015.
22. Becorit GmbH. *Datasheet becorit 929-1*. Germany: Recklinghausen, 1999.
23. CEN. EN 13979-1 Railway applications - wheelsets and bogies - monobloc Wheels - technical approval procedure - Part 1: forged and rolled wheels, *CEN/TC*. 2024.
24. National Instruments Corporation. cDAQTM-9171/9174/9178 User Manual. 2016. https://www.ni.com/docs/en-US/bundle/cdaq-9171-91749178-features/resource/372838e.pdf.
25. LABVIEW. *Labview user manual*. Austin, TX, USA: National Instruments, 2022.
26. FLIR. *X8400sc user manual*. Wilsonville, OR, USA: FLIR, 2013.
27. Sibin KP, John S and Barshilia HC. Control of thermal emittance of stainless steel using sputtered tungsten thin films for solar thermal power applications. *Sol Energy Mater Sol Cell* 2015; 133: 1–7.
28. Sawczuk W. Identification of the hot spots phenomenon in brakes by using a thermal imaging camera. In: Proceedings Quantitative InfraRed Thermography Conference, Gdansk, Poland, July 4-8, 2016.
29. Burstow M, de Podesta M and Pearce J. Identification of the hot spots phenomenon in brakes by using a thermal imaging camera. In: Iwnicki S, (eds), *Proceedings of the 22nd International Symposium on the Dynamics of Vehicles on Roads and on Tracks*, Manchester, UK. 2017.
30. Firlik B, Staśkiewicz T and Słowiński M. Thermal imaging of the wheel-rail interface. *Proc Inst Mech Eng F J Rail Rapid Transit* 2023; 237(9): 1195–1204.
31. Staśkiewicz T, Pawłowski P, Firlik B, et al. Roller rig for wheel-rail wear investigations using thermal imaging. In: Pombo J, (eds.), *Proceedings of the Sixth International Conference on Railway Technology: Research, Development and Maintenance*, Edinburgh, UK, 2024.
32. Debro UMS. *DEBBIE user's manual*. Warsaw, Poland: Debro UMS, 1996.